Enhanced Rotational Motion of Spherical Squirmer in Polymer Solutions

Kai Qi,[1,*] Elmar Westphal,[2,†] Gerhard Gompper,[1,‡] and Roland G. Winkler[1,§]
[1]Theoretical Soft Matter and Biophysics, Institute of Complex Systems and Institute for Advanced Simulation, Forschungszentrum Jülich and JARA, 52425 Jülich, Germany
[2]Peter Grünberg Institute and Jülich Centre for Neutron Science, Forschungszentrum Jülich, D-52425 Jülich, Germany

(Received 16 August 2019; accepted 13 January 2020; published 11 February 2020)

The rotational diffusive motion of a self-propelled, attractive spherical colloid immersed in a solution of self-avoiding polymers is studied by mesoscale hydrodynamic simulations. A drastic enhancement of the rotational diffusion by more than an order of magnitude in the presence of activity is obtained. The amplification is a consequence of two effects, a decrease of the amount of adsorbed polymers by active motion and an asymmetric encounter with polymers on the squirmer surface, which yields an additional torque and random noise for the rotational motion. Our simulations suggest a way to control the rotational dynamics of squirmer-type microswimmers by the degree of polymer adsorption and system heterogeneity.

DOI: 10.1103/PhysRevLett.124.068001

Self-propelled microorganisms are habitually exposed to complex fluid environments [1] consisting of solutions with a broad range of dispersed macromolecules and colloidal particles [2]. However, our current understanding of microorganism locomotion mainly rests upon Newtonian fluids whose properties are governed by viscous stresses, whereas complex fluids are viscoelastic, i.e., they are non-Newtonian, which implies additional elastic effects [3–5]. Potential medical and industrial applications have triggered numerous investigations of the motility of microorganisms in complex fluids, like bacteria swimming and swarming in a biofilm [6] and moving sperm in the reproductive tract [7]. Intuitively, the existence of high-molecular weight macromolecules can be expected to slow down the translational motion of swimmers because of the (substantially) enhanced viscosity [8–11]. However, increased swimming speeds have been reported [4,12–20], where enhancement is attributed to mechanical responses caused by fluid viscoelasticity [4,11,13,14,21], local shear thinning [15,22], and polymer depletion [20,23]. In addition, viscoelasticity affects other microswimmer properties, such as their rotational motion. Recent experimental studies of self-propelled Janus colloids in a viscoelastic fluid yield a drastically enhanced rotational diffusion by up to 2 orders of magnitude [24]. A further increase of activity can even result in persistent rotational motion [25].

In order to shed light onto microscopic mechanisms that lead to an enhanced rotational motion, we perform mesoscale hydrodynamic simulations of a spherical squirmer embedded in a fluid employing the multiparticle collision dynamics (MPC) approach [26,27]. Viscoelasticity is captured by taking linear polymers explicitly into account, which we consider to adsorb on the colloid surface. By variation of the squirmer activity, our simulations yield a drastic enhancement of its rotational diffusion by more than an order of magnitude, in particular in a dilute solution of self-avoiding polymers. This increase is induced by an inhomogeneous distribution of (partially) adsorbed polymers on the squirmer surface moving in the squirmer-induced flow field. Through the adjustment of the squirmer-polymer-interaction strength and system heterogeneity, our results demonstrate the feasibility of controlling the rotational motion of squirmer-type microswimmers in a complex environment.

We consider a squirmer, which is modeled as a neutral buoyant hard sphere of radius ϱ with the prescribed tangential surface slip velocity [28,29],

$$\boldsymbol{u}_{sq} = \frac{3}{2} U_0 \sin(\theta)[1 + \beta \cos(\theta)]\boldsymbol{e}_\theta, \tag{1}$$

where U_0 is the swimming velocity, θ is the polar angle with respect to the squirmer's orientation and swimming direction $\boldsymbol{e}$, $\boldsymbol{e}_\theta$ is the local tangent vector, and β characterizes the active stress ($\beta < 0$ pusher, $\beta = 0$ neutral squirmer, $\beta > 0$ puller); see Fig. 1. The actual flow field of a

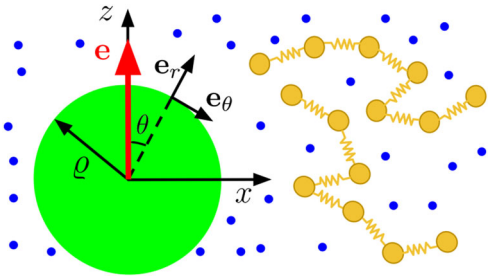

FIG. 1. Sketch for a spherical squirmer of radius ϱ with propulsion direction $\boldsymbol{e}$, radial unit vector $\boldsymbol{e}_r$, and tangential unit vector $\boldsymbol{e}_\theta$ immersed in a viscoelastic fluid of MPC fluid particles (blue dots) and self-avoiding polymers (yellow bead-spring chains).

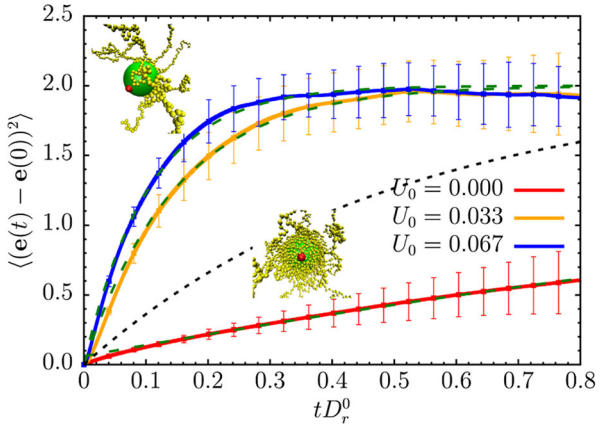

FIG. 2. Rotational mean square displacement (RMSD) of a neutral squirmer, $\beta = 0$, as a function of time for various self-propulsion velocities U_0. Green dashed curves are exponential fits according to Eq. (3), which yields the effective rotational diffusion coefficients $D_r^a \times 10^5/\sqrt{k_BT/ma^2} = 0.47, 7.8, 11$ for $U_0/\sqrt{k_BT/m} = 0, 1/30, 1/15$, respectively. The black dashed line is the RMSD of a squirmer in a simple fluid, with the rotational diffusion coefficient $D_r^0 = 2.3 \times 10^{-5}\sqrt{k_BT/ma^2}$. The error bars indicate the standard deviation. The snapshots illustrate the polymer conformations and distribution. The polymer length is $N_m = 240$, the number of polymers $N_p = 24$, and the monomer packing-fraction ratio $\phi/\phi^* = 0.75$.

swimmer is determined by its particular propulsion mechanism, which for a diffusiophoretic particle depends on the details of the spatial distribution and the type of chemical reactions across its surface [30]. Here, we focus on neutral squirmer, i.e., $\beta = 0$. Results for pushers and pullers are presented in the Supplemental Material (SM) [31].

A linear polymer is composed of N_m touching beads, connected by strong harmonic bonds of finite rest length l_0 (Fig. 1) (cf. SM for details [31]). Polymer excluded-volume interactions are taken into account by a truncated and repulsive Lennard-Jones potential. Polymer adsorption onto the squirmer surface is triggered by the radial, attractive separation-shifted Lennard-Jones-type potential,

$$\frac{U_a(r_a)}{k_BT} = 4\epsilon_a\left[\left(\frac{a}{r_a + 1.377a}\right)^8 - \left(\frac{a}{r_a + 1.377a}\right)^4\right], \quad (2)$$

for monomer-squirmer distances $r_a < 3a$ and zero otherwise, where r_a is the monomer distance with respect to the colloid surface, ϵ_a the attraction strength, and a the length of a MPC collision cell (cf. SM [31]). At the colloid surface, the monomers experience an effective slip velocity due to the tangential squirming velocity of the fluid. The latter can be understood as an effective description of the transport mechanism of ciliated or phoretic microswimmers. A well-known example is the transport of mucus (a viscous polymer gel) by ciliated surfaces in the airways. Similarly, we expect polymer adsorption on colloids to be generic, as for polyacrylamide polymers absorbing on both halves of the silica-carbon Janus particles employed in Ref. [24]. By the coarse-grained nature of our polymer model, every monomer bead corresponds to several molecular segments of a real polymer, with a correspondingly enhanced attraction strength. However, the ratio between colloid diameter 2ϱ and bead size $\sigma \approx l_0$ (typically $2\varrho/l_0 = 12$) is small compared to that of a real colloid and polymer. Nevertheless, the qualitative behavior does not depend significantly on the monomer size, as simulations of systems of phantom polymers with pointlike beads reveal a qualitative similar behavior as of self-avoiding polymers with Lennard-Jones beads.

The squirmer and polymer dynamics is treated by molecular dynamics (MD) simulations, describing the rotational motion of a squirmer by quaternions [29]. For the MPC fluid [26,27], the stochastic-rotation-dynamics variant with angular momentum conservation (MPC-SRD + a) is applied [52]. Details of the implementation and the applied parameters are presented in the SM [31].

We performed between 25 and 50 independent simulation runs of 5×10^6 MPC steps (10^8 MD steps) for every displayed parameter set. Averages, denoted by $\langle\cdots\rangle$, are taken over the various realization and well-separated configurations of individual runs (time average).

Figure 2 displays simulation results for the rotational mean square displacement (RMSD) of the propulsion direction $\boldsymbol{e}$ of a neutral squirmer as a function of time for a system with $N_p = 24$ polymers of length $N_m = 240$ and the packing fraction $\phi/\phi^* = 0.75$. Here, $\phi^* = N_m/V_p$ is the overlap concentration with the polymer volume $V_p = 4\pi R_g^3/3$ in terms of the polymer radius of gyration R_g. Simulations yield $R_g^0/l_0 \approx 11.7$ for $N_m = 240$ at infinite dilution. By fitting the expression

$$\langle[\boldsymbol{e}(t) - \boldsymbol{e}(0)]^2\rangle = 2(1 - e^{-2D_r^a t}), \quad (3)$$

the activity-dependent rotational diffusion coefficient D_r^a can be deduced. The rotational diffusion coefficient of the passive colloid, $D_r^p = 4.7 \times 10^{-6}\sqrt{k_BT/ma^2}$, in the polymer solution is reduced by a factor of 5 compared to that of the colloid in the bare MPC fluid, $D_r^0 = 2.3 \times 10^{-5}\sqrt{k_BT/ma^2}$, reflecting a strong interaction with the polymers. Evidently, activity significantly enhances the rotational diffusion, which we characterize by the rotational diffusion enhancement $\gamma^a = D_r^a/D_r^p$. Our simulations yield the values $\gamma^a = 17$ and $\gamma^a = 23$ for $U_0/\sqrt{k_BT/m} = 1/30$ and $1/15$, respectively.

The short-range attraction implies a substantial monomer increase in the vicinity of the colloid, as illustrated in the SM, Fig. S2 [31], which is the origin of the reduced rotational diffusion of the passive colloid. Activity reduces the monomer concentration, i.e., depletes the polymer next to the squirmer. We attribute this effect to a flow-induced

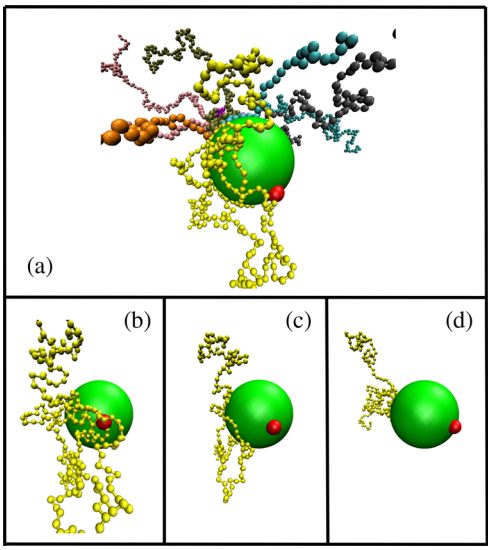

FIG. 3. (a) Snapshot of a neutral squirmer with several adsorbed polymers. The self-propulsion velocity is $U_0/\sqrt{k_BT/m} = 1/15$ and the monomer concentration is $\phi/\phi^* = 0.75$. For a better visualization, adsorbed polymers are displayed with different colors. (b)–(d) Time sequence of the polymer transport and squirmer rotation by the fluid flow. The red dot indicates the squirmer's propulsion direction. See Supplemental Material for an animation [31].

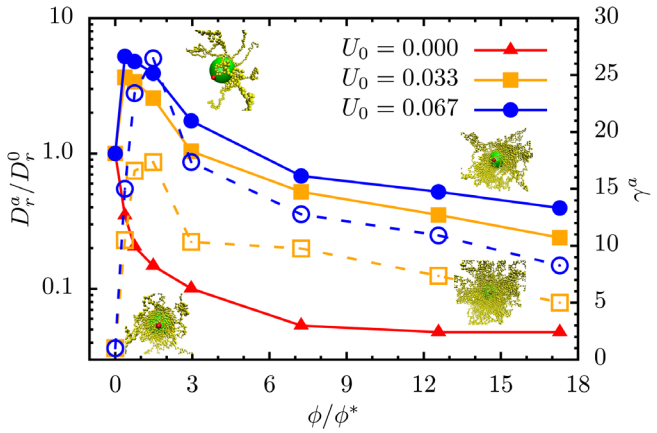

FIG. 4. Normalized rotational diffusion coefficient D_r^a/D_r^0 (solid lines) and its enhancement $\gamma^a = D_r^a/D_r^p$ (dashed lines) as a function of monomer concentration ϕ/ϕ^* for the propulsion strengths $U_0/\sqrt{k_BT/m} = 0$ (triangles), $1/30$ (squares), and $1/15$ (bullets); $\beta = 0$ and $\epsilon_a = 15$. Diffusion coefficients are obtained within 10%–25% accuracy, depending on polymer density.

desorption of polymers by the active colloid motion. Qualitatively, this is similar to experimental [15] and simulation results [20] for bacteria swimming in a viscoelastic fluid and is assumed to be relevant for their observed enhanced swimming speed. Hence, the increase of the rotational diffusion coefficient can be partially attributed to the decreased amount of adsorbed polymers.

The main rotational enhancement is caused by a second effect, the active polymer transport on the colloid surface. The directed active motion along $\boldsymbol{e}$ leads to an asymmetric encounter with the dissolved polymers compared to thermal motion—it is enhanced in the propulsion direction (front). At the same time, the imposed slip velocity [Eq. (1)] causes a transport of the polymer from the front of the colloid to its rear. The polymer transport, together with the required momentum conservation, leads to an enhanced squirmer rotational diffusive motion, as is illustrated in Fig. 3 for a neutral squirmer. In Fig. 3(a), several adsorbed polymers are shown, where the yellow polymer just adsorbs in front. Evidently, the polymer distribution is asymmetric. Figures 3(b)–3(d) illustrate the dynamics of the yellow polymer, which is gradually transported by flow from the front to the rear part of the squirmer. Momentum conservation implies the opposite motion of the whole squirmer, as is visible by the displacement of the red label. Since a squirmer more frequently encounters polymers in front, with no preferential azimuthal angular dependence of absorption, an additional random rotational motion is obtained on top of the rotation by Brownian noise, which enhances the overall rotational diffusion.

This mechanism is most effective as long as the polymer distribution on the squirmer surface is sufficiently low. At high polymer concentrations, the adsorption rate is larger and more homogeneous with a virtually radially symmetric polymer transport on the surface, which restores a symmetric distribution of extra torques and, hence, implies a drop of the activity-enhanced rotational motion. Rotational mean square displacements for a neutral squirmer at various swimming velocities are presented in Fig. 4 as a function of the polymer concentration. (Results for $\beta \neq 0$ are presented and discussed in the SM, Fig. S7 [31].) The data for $U_0 = 0$ indicate the drop of the RMSD by approximately 1 order of magnitude with increasing polymer concentration. In contrast, for $U_0 > 0$, the RMSD increases first with increasing concentration and drops for $\phi/\phi^* \gtrsim 0.38$. At small concentrations, D_r^a is larger than D_r^0 of the colloid in the bare MPC fluid. However, above an activity-dependent concentration, D_r^a drops below D_r^0 ($D_r^a/D_r^0 < 1$ in Fig. 4). The diffusion enhancement $\gamma^a = D_r^a/D_r^0$ is significant for all concentrations, despite the fact that D_r^a drops below D_r^0, because D_r^p decreases stronger with increasing ϕ than D_r^a. As shown in Fig. 4, γ^a assumes values in the range $1 < \gamma^a \lesssim 25$ for the considered propulsion velocities. The maximum values are reached at $\phi/\phi^* \approx 1.5$. At $\phi/\phi^* \approx 17$, the rotational enhancement is still significant, with $\gamma^a \approx 5$ and 8 for $U_0/\sqrt{k_BT/m} = 1/30$ and $1/15$, respectively.

The squirmer locomotion in turn affects the polymer conformations, reflecting the viscoelastic nature of the solution. As shown in Fig. 5, the polymer radius of gyration in the presence of a passive colloid decreases with increasing concentration due to screening of polymer excluded-volume interactions ($R_g^2/(R_g^0)^2 < 1$) [53,54]. In fact, for $\phi/\phi^* \gg 1$, the same concentration dependence is

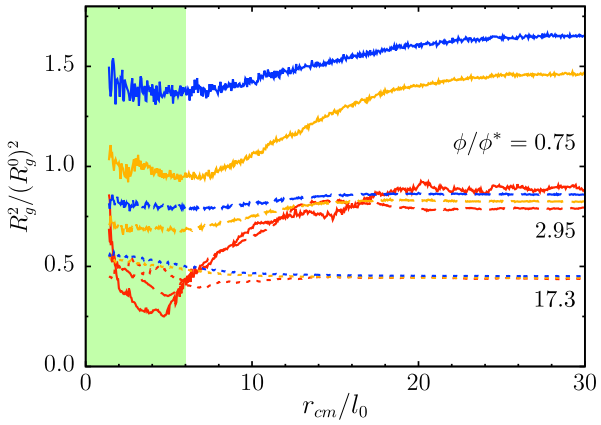

FIG. 5. Polymer radius of gyration R_g^2 scaled by the value at infinite dilution $(R_g^0)^2$ as a function of the radial polymer center-of-mass position $r_{\mathrm{c.m.}}$ from the squirmer center for $U_0/\sqrt{k_BT/m} = 0$ (red), 1/30 (yellow), and 1/15 (blue) and the concentration ratios $\phi/\phi^* = 0.75$ (solid), 2.95 (dashed), and 17.3 (dotted); $\beta = 0$ and $\epsilon_a = 15$. The shaded area indicates polymer center-of-mass positions inside of the squirmer.

obtained, independent of activity (see SM [31]). However, we observe a significant increase in the polymer size at smaller concentrations, $\phi/\phi^* < 3$, which depends on the activity of the squirmer (see also SM, Fig. S3 [31]) [55,56]. Here, due to the limited system size, all polymers are affected. For sufficiently larger system sizes, far from the squirmer, the unperturbed, concentration-dependent equilibrium polymer configuration is assumed (see SM). The latter is visible for higher concentrations, where the polymer conformations are rather similar for all activities. In the vicinity of a surface, the radius of gyration of a polymer decreases with decreasing distance from the surface, where surface attraction substantially enhances the effect, whereas activity reduces compactification. By wrapping around the squirmer, the polymer center of mass can be located inside the colloid. Center-of-mass distances $r_{\mathrm{c.m.}}/\varrho \ll 1$ appear for rather deformed polymers, where the radius of gyration increases again.

Our results indicate a major influence of the polymeric nature of the adsorbed object on the enhancement of the rotational diffusion of squirmers, because simulations of monomers only yield approximately the same squirmer rotational diffusion as obtained for a bare MPC fluid, despite strong monomer adsorption and active transport (cf. SM for results of polymers with $N_m = 60$ [31]).

A significant larger enhancement of the rotational diffusion coefficient has been obtained in the experiments of Ref. [24] for Janus particles in polymer solutions. This could be related to the larger size ratio of the Janus particle and polymer radius of gyration in the experiment compared to the current simulation study. In fact, in experiments, the rotational diffusion coefficient of the passive Janus colloid in the polymer solution is by a factor of approximately 30 smaller than that of the colloid in the bare binary mixture, while in our case, the factor is approximately 5 at $\phi/\phi^* = 0.75$. Hence, a possible depletion of polymer in the vicinity of the colloid by activity would already imply a significantly larger rotational diffusion in experiments than in simulations.

In Ref. [25], the rotational enhancement is attributed to memory effects of the viscoelastic fluid, where an internal force nonaligned with the actual squirmer orientation emerges in a coarse-grained continuum "macroscopic" description. In simulations, we find concentration-dependent reduced swimming velocities on the order of 40%, but the swimming direction is closely aligned with the propulsion direction. Hence, we cannot explain the observed effect by misalignment of propulsion and swimming direction.

In our microscopic simulations, rotational enhancement of neutral squirmers originates from two effects: (i) reduction of the amount of adsorbed polymers by activity compared to that of a passive colloid—implying an increase in the rotational diffusion coefficient—and (ii) an asymmetric encounter of the squirmer with polymers at the front leading to an additional torque by the surface fluid flow, which yields an additional random contribution to the rotational motion. We would like to emphasize that the polymer character of the solute is important and that the rotation enhancement depends on polymer length as shown in the SM [31]. In particular, we do not observe an enhancement for a pure monomer solution.

Various other scenarios of colloid-polymer interactions are possible: local attachment with finite lifetime, temporary local attachment on various patches, local permanent attachment, or even active stress-induced hydrodynamic accumulation ($|\beta| > 0$). We present results for the latter two cases in the SM. For a few locally bound beads, which are not transported by the surface flow field, we find a continuous rotational motion opposite to the case of homogeneous attraction, and the squirmer propagates along circular trajectories reminiscent of those observed in Ref. [25]. Sufficiently strong pusher flow fields lead to an enhanced polymer accumulation, which amplifies the rotational diffusive motion (cf. SM for more details [31]).

The flow field of a phoretic Janus particle is well described by a squirmer-type model employing a phoretic-slip hydrodynamic boundary condition, equivalent to our approach, however, with a somewhat different flow field [30,57]. Hence, the proposed monomer transport by surface slip may also be relevant for Janus particles. Differences in adsorption affinity of the two materials, however, may lead a preferred adsorption of the polymer to one of them. This could lead to pinning of a polymer at their interface line, and consequently to a rotation as emerging by our pinned polymer. Here, further studies taking into account the Janus-type structured colloidal

surfaces are desirable, which can be performed by our modeling approach.

Our simulations suggest a possible mechanism to modify and control the rotational motion of an active colloid with slip velocity in polymer solutions. In particular, they emphasize the importance of an inhomogeneous and anisotropic squirmer-polymer interaction. Further studies are necessary to resolve the actual mechanism in experiments, with a rather complex interplay of phoretic flow fields and polymer colloid interactions.

This work has been supported by the DFG priority program SPP 1726 "Microswimmers from Single Particle Motion to Collective Behaviour." The authors gratefully acknowledge the computing time granted through Jülich Aachen Research Alliance—High-Performance Computing (JARA-HPC) on the supercomputer JURECA at Forschungszentrum Jülich.

*k.qi@fz-juelich.de
†e.westphal@fz-juelich.de
‡g.gompper@fz-juelich.de
§r.winkler@fz-juelich.de

[1] J. Elgeti, R. G. Winkler, and G. Gompper, Physics of microswimmers—single particle motion and collective behavior: a review, Rep. Prog. Phys. **78**, 056601 (2015).
[2] M. A. McGuckin, S. K. Lindén, P. Sutton, and T. H. Florin, Mucin dynamics and enteric pathogens, Nat. Rev. Microbiol. **9**, 265 (2011)..
[3] E. Lauga, Propulsion in a viscoelastic fluid, Phys. Fluids **19**, 083104 (2007).
[4] A. Patteson, A. Gopinath, M. Goulian, and P. E. Arratia, Running and tumbling with E. coli in polymeric solutions, Sci. Rep. **5**, 15761 (2015).
[5] T. Qiu, T.-C. Lee, A. G. Mark, K. I. Morozov, R. Münster, O. Mierka, S. Turek, A. M. Leshansky, and P. Fischer, Swimming by reciprocal motion at low Reynolds number, Nat. Commun. **5**, 5119 (2014).
[6] A. Houry, M. Gohar, J. Deschamps, E. Tischenko, S. Aymerich, A. Gruss, and R. Briandet, Bacterial swimmers that infiltrate and take over the biofilm matrix, Proc. Natl. Acad. Sci. U.S.A. **109**, 13088 (2012).
[7] L. J. Fauci and R. Dillon, Biofluidmechanics of reproduction, Annu. Rev. Fluid Mech. **38**, 371 (2006).
[8] X. N. Shen and P. E. Arratia, Undulatory Swimming in Viscoelastic Fluids, Phys. Rev. Lett. **106**, 208101 (2011).
[9] L. Zhu, E. Lauga, and L. Brandt, Self-propulsion in viscoelastic fluids: Pushers vs. pullers, Phys. Fluids **24**, 051902 (2012).
[10] B. Qin, A. Gopinath, J. Yang, J. P. Gollub, and P. E. Arratia, Flagellar kinematics and swimming of algal cells in viscoelastic fluids, Sci. Rep. **5**, 9190 (2015).
[11] C. Datt, G. Natale, S. G. Hatzikiriakos, and G. J. Elfring, An active particle in a complex fluid, J. Fluid Mech. **823**, 675 (2017).
[12] H. C. Berg and L. Turner, Movement of microorganisms in viscous environments, Nature (London) **278**, 349 (1979).
[13] J. Teran, L. Fauci, and M. Shelley, Viscoelastic Fluid Response Can Increase the Speed and Efficiency of a Free Swimmer, Phys. Rev. Lett. **104**, 038101 (2010).
[14] J. Espinosa-Garcia, E. Lauga, and R. Zenit, Fluid elasticity increases the locomotion of flexible swimmers, Phys. Fluids **25**, 031701 (2013).
[15] V. A. Martinez, J. Schwarz-Linek, M. Reufer, L. G. Wilson, A. N. Morozov, and W. C. K. Poon, Flagellated bacterial motility in polymer solutions, Proc. Natl. Acad. Sci. U.S.A. **111**, 17771 (2014).
[16] S. Jung, Caenorhabditis elegans swimming in a saturated particulate system, Phys. Fluids **22**, 031903 (2010).
[17] A. M. Leshansky, Enhanced low-Reynolds-number propulsion in heterogeneous viscous environments, Phys. Rev. E **80**, 051911 (2009).
[18] S. Gómez, F. A. Godínez, E. Lauga, and R. Zenit, Helical propulsion in shear-thinning fluids, J. Fluid Mech. **812**, R3 (2017).
[19] Y. Magariyama and S. Kudo, A mathematical explanation of an increase in bacterial swimming speed with viscosity in linear-polymer solutions, Biophys. J. **83**, 733 (2002).
[20] A. Zöttl and J. M. Yeomans, Enhanced bacterial swimming speeds in macromolecular polymer solutions, Nat. Phys. **15**, 554 (2019).
[21] E. E. Riley and E. Lauga, Enhanced active swimming in viscoelastic fluids, Europhys. Lett. **108**, 34003 (2014).
[22] S. E. Spagnolie, B. Liu, and T. R. Powers, Locomotion of Helical Bodies in Viscoelastic Fluids: Enhanced Swimming at Large Helical Amplitudes, Phys. Rev. Lett. **111**, 068101 (2013).
[23] Y. Man and E. Lauga, Phase-separation models for swimming enhancement in complex fluids, Phys. Rev. E **92**, 023004 (2015).
[24] J. R. Gomez-Solano, A. Blokhuis, and C. Bechinger, Dynamics of Self-Propelled Janus Particles in Viscoelastic Fluids, Phys. Rev. Lett. **116**, 138301 (2016).
[25] N. Narinder, C. Bechinger, and J. R. Gomez-Solano, Memory-Induced Transition from a Persistent Random Walk to Circular Motion for Achiral Microswimmers, Phys. Rev. Lett. **121**, 078003 (2018).
[26] R. Kapral, Multiparticle collision dynamics: Simulation of complex systems on mesoscales, Adv. Chem. Phys. **140**, 89 (2008).
[27] G. Gompper, T. Ihle, D. M. Kroll, and R. G. Winkler, Multiparticle collision dynamics: A particle-based mesoscale simulation approach to the hydrodynamics of complex fluids, Adv. Polym. Sci. **221**, 1 (2009).
[28] T. Ishikawa, M. Simmonds, and T. J. Pedley, Hydrodynamic interaction of two swimming model micro-organisms, J. Fluid Mech. **568**, 119 (2006).
[29] M. Theers, E. Westphal, G. Gompper, and R. G. Winkler, Modeling a spheroidal microswimmer and cooperative swimming in a narrow slit, Soft Matter **12**, 7372 (2016).
[30] M. N. Popescu, W. E. Uspal, Z. Eskandari, M. Tasinkevych, and S. Dietrich, Effective squirmer models for self-phoretic chemically active spherical colloids, Eur. Phys. J. E **41**, 145 (2018).
[31] See Supplemental Material at http://link.aps.org/supplemental/10.1103/PhysRevLett.124.068001 for a detailed description of the MPC approach, the polymer model,

the implemenation of the squirmer and the polymers in MPC, additional results for polymers with $N_m = 250$ and 60 monomers, results on the effect of active stress ($\beta \neq 0$) on polymer adsorption and the rotational diffusion coefficient, results on the squirmer rotational motion for various tightly bound monomers, and descriptions of movies from simulations, which includes Refs. [32–51].

[32] A. Malevanets and R. Kapral, Mesoscopic model for solvent dynamics, J. Chem. Phys. **110**, 8605 (1999).

[33] M. Theers, E. Westphal, K. Qi, R. G. Winkler, and G. Gompper, Clustering of microswimmers: Interplay of shape and hydrodynamics, Soft Matter **14**, 8590 (2018).

[34] T. Ihle and D. M. Kroll, Stochastic rotation dynamics: A Galilean-invariant mesoscopic model for fluid flow, Phys. Rev. E **63**, 020201(R) (2001).

[35] H. Noguchi and G. Gompper, Transport coefficients of off-lattice mesoscale-hydrodynamics simulation techniques, Phys. Rev. E **78**, 016706 (2008).

[36] M. Yang, M. Theers, J. Hu, G. Gompper, R. G. Winkler, and M. Ripoll, Effect of angular momentum conservation on hydrodynamic simulations of colloids, Phys. Rev. E **92**, 013301 (2015).

[37] M. Theers and R. G. Winkler, Bulk viscosity of multiparticle collision dynamics fluids, Phys. Rev. E **91**, 033309 (2015).

[38] T. Ihle and D. M. Kroll, Stochastic rotation dynamics I: Formalism, Galilean invariance, Green-Kubo relations, Phys. Rev. E **67**, 066705 (2003).

[39] C.-C. Huang, A. Varghese, G. Gompper, and R. G. Winkler, Thermostat for nonequilibrium multiparticle-collision-dynamics simulations, Phys. Rev. E **91**, 013310 (2015).

[40] T. Ihle, Chapman-Enskog expansion for multi-particle collision models, Phys. Chem. Chem. Phys. **11**, 9667 (2009).

[41] C.-C. Huang, G. Gompper, and R. G. Winkler, Hydrodynamic correlations in multiparticle collision dynamics fluids, Phys. Rev. E **86**, 056711 (2012).

[42] K. Mussawisade, M. Ripoll, R. G. Winkler, and G. Gompper, Dynamics of polymers in a particle based mesoscopic solvent, J. Chem. Phys. **123**, 144905 (2005).

[43] A. Malevanets and J. M. Yeomans, Dynamics of short polymer chains in solution, Europhys. Lett. **52**, 231 (2000).

[44] C.-C. Huang, A. Chatterji, G. Sutmann, G. Gompper, and R. G. Winkler, Cell-level canonical sampling by velocity scaling for multiparticle collision dynamics simulations, J. Comput. Phys. **229**, 168 (2010).

[45] C. C. Huang, G. Gompper, and R. G. Winkler, Effect of hydrodynamic correlations on the dynamics of polymers in dilute solution, J. Chem. Phys. **138**, 144902 (2013).

[46] M. P. Allen and D. J. Tildesley, *Computer Simulation of Liquids* (Clarendon Press, Oxford, 1987).

[47] J. T. Padding, A. Wysocki, H. Löwen, and A. A. Louis, Stick boundary conditions and rotational velocity auto-correlation functions for colloidal particles in a coarse-grained representation of the solvent, J. Phys. Condens. Matter **17**, S3393 (2005).

[48] A. Lamura, G. Gompper, T. Ihle, and D. M. Kroll, Multi-particle collision dynamics: Flow around a circular and a square cylinder, Europhys. Lett. **56**, 319 (2001).

[49] I. P. Omelyan, Algorithm for numerical integration of the rigid-body equations of motion, Phys. Rev. E **58**, 1169 (1998).

[50] M. Ripoll, K. Mussawisade, R. G. Winkler, and G. Gompper, Dynamic regimes of fluids simulated by multiparticle-collision dynamics, Phys. Rev. E **72**, 016701 (2005).

[51] J. Hu, M. Yang, G. Gompper, and R. G. Winkler, Modelling the mechanics and hydrodynamics of swimming E. coli, Soft Matter **11**, 7843 (2015).

[52] M. Theers, E. Westphal, G. Gompper, and R. G. Winkler, From local to hydrodynamic friction in Brownian motion: A multiparticle collision dynamics simulation study, Phys. Rev. E **93**, 032604 (2016).

[53] M. Doi and S. F. Edwards, *The Theory of Polymer Dynamics* (Clarendon Press, Oxford, 1986).

[54] C.-C. Huang, R. G. Winkler, G. Sutmann, and G. Gompper, Semidilute polymer solutions at equilibrium and under shear flow, Macromolecules **43**, 10107 (2010).

[55] T. Eisenstecken, G. Gompper, and R. G. Winkler, Conformational properties of active semiflexible polymers, Polymers **8**, 304 (2016).

[56] R. G. Winkler, J. Elgeti, and G. Gompper, Active polymers—Emergent conformational and dynamical properties: A brief review, J. Phys. Soc. Jpn. **86**, 101014 (2017).

[57] S. Michelin and E. Lauga, Phoretic self-propulsion at finite Péclet numbers, J. Fluid Mech. **747**, 572 (2014).